applied sciences

MDPI

Article

Fluid-Solid Coupling Effect on Numerical Simulation of Deep Foundation Pit Deformation in Soft Soil Area

Yu Zhang [1,*], Zuodong Jin [1], Yunlong Hou [2], Bingbing Han [2] and Charles Ntakiyimana [1]

[1] School of Traffic and Transportation, Lanzhou Jiaotong University, Lanzhou 730070, China
[2] Gansu Institute of Engineering Geology, Lanzhou 730030, China
* Correspondence: zhangyu@mail.lzjtu.cn

Abstract: Groundwater is abundant in soft soil areas, which has a significant impact on the excavation deformation of foundation pits. In this paper, based on the monitoring of deep foundation pits with waterproof curtains in Shanghai deep foundation pits, COMSOL Multiphysics is used to model the layers of the foundation pits and establish a two-dimensional seepage-consolidation coupled model for hierarchical dewatering excavation. The feasibility of numerical simulation of regional foundation pits, the modeling method of the foundation pit seepage model is explored, and the presence or absence of waterproof curtains, and the influence of aquitards on the horizontal displacement of foundation pits and surface settlement outside the pits is analyzed. The research shows that the simulated foundation pit deformation values are in good agreement with the actual monitoring values and that the effect of dewatering and seepage has a great influence on the foundation pit deformation. The waterproof curtain has a significant effect on reducing the drop in the water level outside the pit and controlling the surface settlement. After installing a waterproof curtain, the amount of ground settlement is reduced, but the disadvantage is that the deformation of the enclosure structure increases. Finally, the influence of aquitard on the deformation of foundation pit excavation is simulated, and the distribution characteristics of the flow network diagram under different permeability coefficients are analyzed. According to the analysis of the foundation pit deformation law and flow network diagram, it is considered that the waterproof curtain can effectively reduce the influence of aquitard on foundation pit deformation.

Keywords: soft soil area; fluid-solid coupling; horizontal displacement; settlement; waterproof curtain; aquitard

check for updates

Citation: Zhang, Y.; Jin, Z.; Hou, Y.; Han, B.; Ntakiyimana, C. Fluid-Solid Coupling Effect on Numerical Simulation of Deep Foundation Pit Deformation in Soft Soil Area. *Appl. Sci.* **2022**, *12*, 11242. https://doi.org/10.3390/app122111242

Academic Editors: Zhenhao Zhang, Yi Zhang, Dixiong Yang and Sifeng Bi

Received: 4 October 2022
Accepted: 4 November 2022
Published: 6 November 2022

Publisher's Note: MDPI stays neutral with regard to jurisdictional claims in published maps and institutional affiliations.

Copyright: © 2022 by the authors. Licensee MDPI, Basel, Switzerland. This article is an open access article distributed under the terms and conditions of the Creative Commons Attribution (CC BY) license (https://creativecommons.org/licenses/by/4.0/).

1. Introduction

The safety of excavations for deep foundation works is an important issue in urban construction, especially for deep foundation pits next to urban roads and buildings [1,2]. Deep foundation pits, especially in soft soil areas, which are characterized by low soil strength and a high water table, are more prone to engineering problems. Seepage research in subterranean spaces is already advanced [3,4], but not effectively integrated with pit safety. Some researchers have proposed predictions for building safety problems through probabilistic prediction methods, but the models are more macroscopic [5,6]. In order to control the horizontal displacement and subgrade settlement, to ensure the safety of personnel, and to reduce engineering losses, the monitoring of deep pits and the numerical simulation of fluid-solid coupling are very important. Liu et al. [7] used the finite element method to analyze the fluid-solid coupling process of the multi-level cascade dewatering excavation process based on the Biot consolidation theory. Xue et al. [8] designed a seepage model test device and conducted a groundwater seepage simulation test on the suspended curtain foundation pit, obtained the seepage flow network shape consistent with the actual project, and studied the characteristics and laws of the groundwater seepage field. Zhang et al. [9] considered the influence of the soil void ratio and compressibility index

changes caused by the drop in groundwater level on the calculation of land subsidence and proposed a calculation method for ground subsidence outside the pit caused by dewatering in the foundation pit in the aquifer at different insertion depths of the waterproof curtain. Chen et al. [10] conducted a finite element numerical simulation to analyze the deformation of the foundation pit and adjacent pipelines under the dewatering excavation of the foundation pit and studied the deformation response of the foundation pit and adjacent pipelines when the waterproof curtain was inserted at different depths under steady seepage. Shen et al. [11] calculated the groundwater flow in three-dimensional conditions and soil deformation in one-dimensional conditions and analyzed the relationships among land subsidence, groundwater withdrawal volume, and groundwater level.

In water-rich areas, the groundwater control system usually adopts the dewatering method of setting up pumping wells in the foundation pit to ensure construction safety [12,13]. However, dewatering will cause groundwater to fall and retaining walls to move [14,15], which, in combination, can lead to severe land subsidence. In the calculation of the horizontal displacement of the envelope structure, the effect of seepage is often ignored [16]. The effect of a waterproof curtain on the aquitard is rarely mentioned [17,18]. Some scholars have simulated the seepage field of deep foundation pits and calculated the settlement during precipitation [19–27].

This paper uses COMSOL Multiphysics to simulate the excavation process of the foundation pit, a deep foundation pit project in Shanghai. Compare the simulated data and the measured data, verify the accuracy of the fluid-solid coupling model, explore and analyze the role of the waterproof curtain in the deformation control of the foundation pit, and examine the influence of the permeability coefficient of the aquitard on the deformation of the foundation pit.

2. Engineering Background and Model

2.1. Engineering Background

The foundation pit is located in the North Bund area of Yangshupu Road, Hongkou District, Shanghai, with the Huangpu River in the south, Yangshupu Road in the north, and Ruifeng Building and Qinhuangdao Road in the east. The foundation pit is surrounded by bored cast-in-place piles, on which concrete support is used, and a three-axis cement-soil mixing pile with a diameter of 850 mm is used as a waterproof curtain. The pit is irregularly rectangular in shape, measuring approximately 230 m from east to west and 140 m from north to south. The excavation depth of the foundation pit is 13.4 m, which belongs to the category of deep foundation pit.

In the parameter design, the excavation depth of the foundation pit is 13.4 m, with the center point of the pit bottom as the center and the vertical direction as the symmetry axis, and half of the foundation pit is selected as the research object. According to local hydrological materials, it is assumed that the water level height of the foundation pit is 2 m underground, and it is assumed that the influence of the water level is not considered when the distance from the foundation pit is more than three times.

2.2. Model and Meshing

The vertical influence depth is generally greater than or equal to 2 times the depth of the foundation pit, while the horizontal influence range is generally greater than or equal to 3 times the depth of the foundation pit. Since the excavation depth of the foundation pit is 13.4 m, the depth of this model is 40 m, and the horizontal distance is 60 m.

Comsol is used in this work, it is a commercially available software based on the low order finite element method. In this regard, based on a better accuracy and calculation time considerations, the spectral element method (SEM) can be selected for use due to its ultimate accuracy [28,29]. The meshing of the model is shown in Figure 1. The meshing must take into account the accuracy of the calculation and the calculation time. The bored pile is used as the key part of the mesh, as the center of the mapping, and spreads out to the remaining parts, forming a meshing with the key points of the calculation spreading

outward. Such a division increases the accuracy of the critical part of the calculation and effectively reduces the calculation time, as shown in Wu [14] and Yazgan [30].

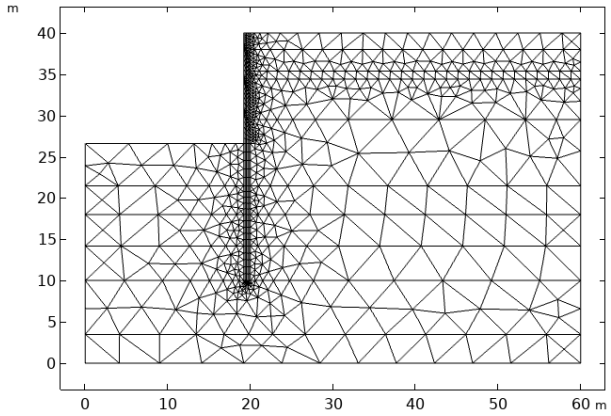


Figure 1. Model meshing diagram.

When the effects of seepage and pore water pressure are not considered, the main factors affecting the horizontal displacement of bored piles are the uniform load and soil plasticity in the upper part of the foundation pit. The uniform load of 35×10^3 Pa in the upper part of the foundation pit and the soil plasticity are calculated by matching the Mohr–Coulomb criterion with the D-P criterion.

In addition, the modeling approach for the pit seepage model is explored. The most critical aspect is the determination of the water table height. Firstly, the water head of the soil in the pit needs to be determined. In the setting of the boundary conditions, the water head of the DE should be kept consistent and constant with the water table height in the area. Prior to construction, water should be precipitated, and generally, the water table height line after precipitation should meet less than 0.5 m above the excavation depth. Therefore, the water heads in AC and AB should be equal to the water table height after precipitation. Finally, the process of precipitation is simulated by the change in water head in the precipitation well [9].

2.3. Material Parameters

We simulated the horizontal displacement and surface settlement of the bored pile after excavation of the foundation pit by using COMSOL Multiphysics. The model is stratified by referring to the geological structure stratification in Table 1. The fourth layer (silty clay) in Table 1 is a weakly permeable layer. The depths range from 10.5 to 18.5 m.

Table 1. Mechanical parameters of soil.

Number	Hydrogeology	Depth (m)	Thickness (m)	Unit Weight (kN/m^{-3})	Shear Experiment		Poisson's Ratio
					Cohesion (kPa)	Internal Friction Angle (°)	
1	Filled soil	/	4.6	18	0	10	0.3
2	Clay sand	4.6	1	18.2	10	29	0.25
3	Silt sandy clay	5.6	4.9	17.4	14	18	0.25
4	Silty clay	10.5	8	16.9	14	11	0.25
5	Clay	18.5	3.5	17.8	19	12.5	0.25
6	Silty clay	22.3	3.8	18.1	20	19	0.25
7	Sandy clay	26.5	4.2	19.9	50	19.5	0.25
8	Sandy silts	30.7	6.5	18.7	3	35.5	0.25
9	Sand	37.2	13.8	18.7	1	36	0.25

2.4. Supporting Structure Parameters

The strength grade of the bored pile is C30, the Young's modulus is 30 MPa, and the Poisson's ratio is 0.3. The pit is supported in three layers, set at depths of −2 m, −6 m,

and −10 m, with four meters between supports. The inner supporting structure adopts steel pipe struts, the maximum allowable displacement of the prestressed bolt is set to 25 mm, and the Young's modulus is 2×10^5 Mpa. When the displacement is less than the allowable displacement, the bolt does not apply supporting force. When the displacement is greater than 25 mm, the supporting force will increase linearly with the increase of displacement. The strength parameters of the three-layer supporting structure are equal. When the excavation reaches a certain depth, the columns are activated as long as the deflection of the bored pile is greater than the allowable value.

The axial stiffness S of the supporting structure is estimated as:

$$S = E\frac{A}{l} \tag{1}$$

A is the cross-sectional area, l is the length of the support, and E is the Young's modulus of the material.

2.5. Fluid-Solid Coupling Theory

The coastal areas of China belong to the soft soil areas. The change of the underground pressure head in the soft soil will lead to elastic-plastic deformation, and during the excavation of the foundation pit with a waterproof curtain, the excavation of the foundation pit will cause the difference of the water head inside and outside the pit.

The deformation of a saturated porous medium caused by fluid withdrawal is theoretically described by the three-dimensional fully coupled poroelasticity model [31]. The theory considers the stress-strain relationship between the fluid and the solid skeleton and its mode of motion separately [32].

The complex situation is better reflected in the calculation of the Biot consolidation theory [7,33]. Biot theory presents a three-dimensional, fully coupled pore elastic model, which is widely used in calculations for numerical simulations. The Biot theory assumes that all layers around the pit are homogeneous, fully saturated, and that the soil particles and pore water are incompressible and describes the deformation of saturated porous media caused by fluid withdrawal under Darcy's law [34] and is applicable to the problem of deformation of porous media caused by the process of foundation pit precipitation. The groundwater seepage in the model follows Darcy's theorem. Based on Biot's consolidation theory, the two-dimensional fluid-solid coupling equation can be expressed as:

$$-G\nabla^2 w_x - \frac{G}{1-2v}\cdot\frac{\partial}{\partial_x}\left(\frac{\partial w_x}{\partial_x}+\frac{\partial w_y}{\partial_y}\right)+\frac{\partial u}{\partial_x}=0 \tag{2}$$

$$-G\nabla^2 w_y - \frac{G}{1-2v}\cdot\frac{\partial}{\partial_y}\left(\frac{\partial w_x}{\partial_x}+\frac{\partial w_y}{\partial_y}\right)+\frac{\partial u}{\partial_y}=-\gamma_t \tag{3}$$

$$-\frac{\partial}{\partial_t}\left(\frac{\partial w_x}{\partial_x}+\frac{\partial w_y}{\partial_y}\right)+\frac{1}{\gamma_w}\left\{\frac{\partial}{\partial_x}\left(k_x\cdot\frac{\partial u}{\partial_x}\right)+\frac{\partial}{\partial_y}\left[k_y\left(\frac{\partial u}{\partial_y}+\gamma_w\right)\right]\right\}=0 \tag{4}$$

G is Young's modulus; ∇^2 is Laplace operator; w_x, w_y refer to the displacement along the x, y direction; v is Poisson's ratio; u is pore water pressure; γ_t, γ_w are the unit weight of soil and water; k_x, k_y refer to the permeability coefficient along the x, y direction.

Calculation method: According to study [12], the yield criterion of the soil around the pit needs to be determined first, and in this paper the Moore–Coulomb criterion is used to calculate the stress-strain of the soil in different layers. Boundary conditions and initial pore water pressure conditions are set, parameters are input, and meshing is carried out before the calculation.

3. Numerical Simulation of Foundation Pit Deformation

For the calculation of the horizontal displacement of the foundation pit, the influence of gravity can be ignored, while in the calculation of the settlement and uplift of the foundation

pit, the prestressing effect of gravity and the process of unloading the foundation pit need to be considered. The difference between the non-fluid-solid coupling model and the fluid-solid coupling model is whether the pore pressure changes due to the dewatering process are taken into account. The soil around the pit is used as a viscoelastic material and the strength is calculated based on M-C criterion and D-P criterion [35].

$$-G\nabla^2 w_x - \frac{G}{1-2v}\cdot\frac{\partial}{\partial_x}\left(\frac{\partial w_x}{\partial_x}+\frac{\partial w_y}{\partial_y}\right)=0 \tag{5}$$

$$-G\nabla^2 w_y - \frac{G}{1-2v}\cdot\frac{\partial}{\partial_y}\left(\frac{\partial w_x}{\partial_x}+\frac{\partial w_y}{\partial_y}\right)=-\gamma_t \tag{6}$$

$$-\frac{\partial}{\partial_t}\left(\frac{\partial w_x}{\partial_x}+\frac{\partial w_y}{\partial_y}\right)+\frac{1}{\gamma_w}\frac{\partial}{\partial_y}\left(k_y\gamma_w\right)=0 \tag{7}$$

In the non-fluid-solid coupling model, the dewatering process during the excavation of the foundation pit is not considered. Therefore, the consolidation settlement caused by dewatering is not considered.

3.1. Horizontal Displacement of the Enclosure

Use CX-3 soil inclinometer to monitor the horizontal displacement of the enclosure. The calculated and measured values of the horizontal displacement of the bored pile are shown in Figure 2. The maximum displacement calculated by the fluid-solid coupling model is −23.3 mm, which appears at the buried depth of −9.7 m. The maximum value of the calculated value of non-fluid-solid coupling is 14.9 mm, which appears at the buried depth of −10.4 m. The maximum monitoring displacement is −23.2 mm, which occurs at the buried depth of −11 m. The maximum displacement calculated by the fluid-solid coupling model is closer to the actual value, and the position of the maximum displacement point calculated by the two models is relatively close to the actual position. In general, the fluid-solid model is better.

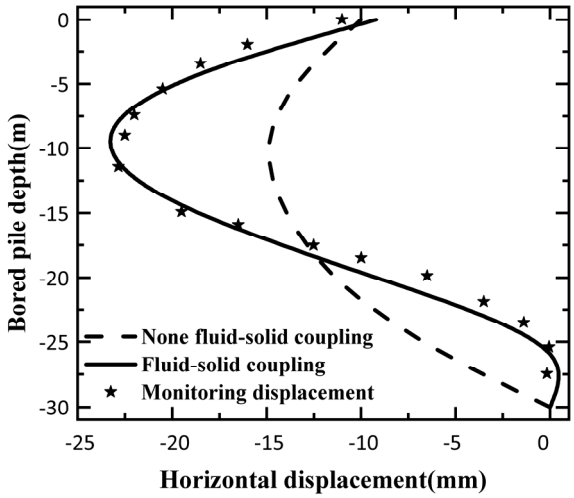


Figure 2. Comparison of calculated and measured values of horizontal displacement of bored piles.

3.2. Internal Force Analysis of Enclosure Structure

Khatri's finite element analysis of the bearing capacity of axially-loaded piles in clay based on the von Mises yield criterion, which compares well with actual test results. The von Mises yield criterion is more accurate and closer to the experimental values than the Moore–Coulomb criterion for the calculation of stresses in piles [36,37]. Chakraborty [38] also applied the von Mises yield criterion to obtain a satisfactory result. The finite element simulation of the von Mises stress of the bored pile is carried out, and the variation of the von Mises stress with the depth of the bored pile is shown in Figure 3. It is clear

from Figure 3 that the two trends are relatively similar, but the maximum stress at the same depth is very different. The results of the fluid-solid coupling calculations are significantly larger. This is due to the constraints of the model, which constrain the horizontal displacement between the top and bottom of the bored pile. The non-fluid-solid coupling model maximum is at −9.9 m, while the fluid-solid coupling model maximum is at −8.4 m, presumably the effect of seepage, with pore stresses accounting for a greater proportion of the depth of the pit excavation. Considering the seepage and dewatering, the stress of the bored-in-place piles inside the pit increases significantly.

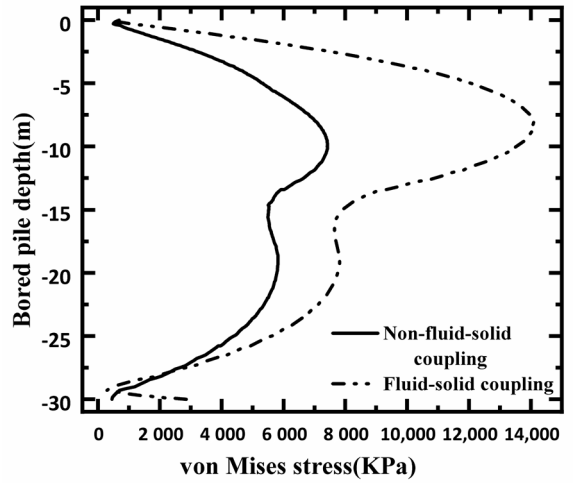


Figure 3. Von Mises stress diagram of bored pile.

The shear stress diagram is shown in Figure 4. It can be found that after considering the effect of dewatering and fluid-solid coupling, the shear stress of the bored piles generally increases, and the shear stress appears at −2 m, −6 m, −10 m at the buried depth of the pile. 242.9 kPa, appearing at −1.9 m buried depth. The depth of the sudden change point is the set depth of the support structure. It is inferred that the sudden change of shear stress is caused by the force of the inner support. Due to the lateral displacement of the bored pile, the compression of the inner support gives the pile an opposite force. Secondly, the pile body also has a sudden change point at the depth of the pit bottom, which is analyzed as an uneven force caused by the empty condition of the excavation of the foundation pit. Therefore, the key parts of pile body shear resistance are the junction of the pit bottom and the pile body and the joint part of the supporting steel pipe and the bored pile, and the monitoring and protection of the shear strength at this point should be strengthened.

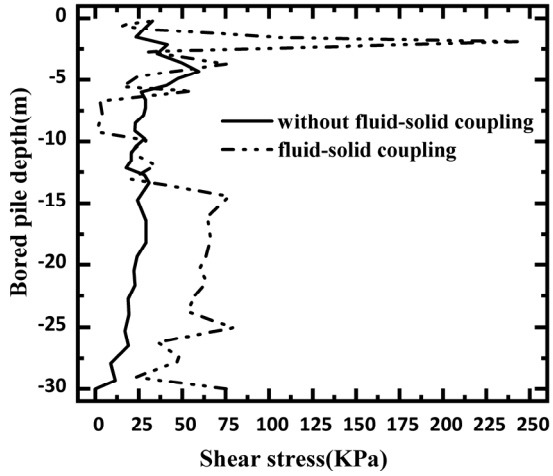


Figure 4. Shear stress diagram of bored pile.

4. Influence of Waterproof Curtain on Deformation of Foundation Pit

The simulation of the water barrier is achieved by changing the infiltration coefficient in the model. To differentiate significantly, the bored piles do not pass water when there is a water barrier. The seepage field is calculated by the porosity of the cement when there is no water barrier. According to Wang's research [39], combined with the actual water-cement ratio used in the project, the porosity of the bored pile is taken to be 0.108. After installing the waterproof curtain, due to the difference in water head height inside and outside the pit, the pore pressure from outside the pit to the inside of the pit is generated, which leads to an increase in the deformation of the enclosure structure. Figures 5 and 6 show the variation of horizontal displacement versus settlement for different models. The maximum settlement is 12.5 mm with the waterproof curtain, and 30.7 mm without the waterproof curtain. The maximum settlement occurred at 10 m away from the foundation pit. The maximum horizontal displacement of the case with waterproof curtain is 22.7 mm, and the maximum settlement of the case without waterproof curtain is 20.6 mm. All occurred at the buried depth of −12.5 m.

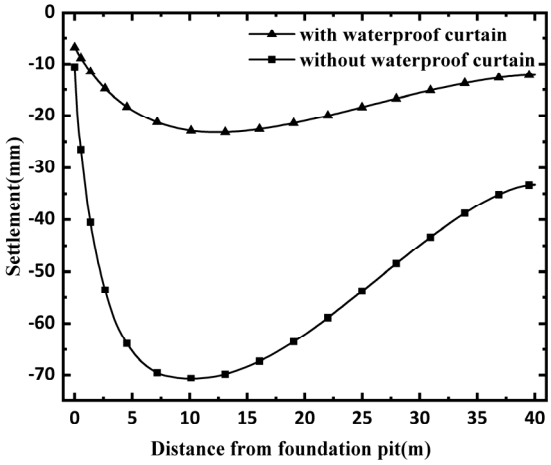


Figure 5. Influence of waterproof curtain on surface settlement outside the pit.

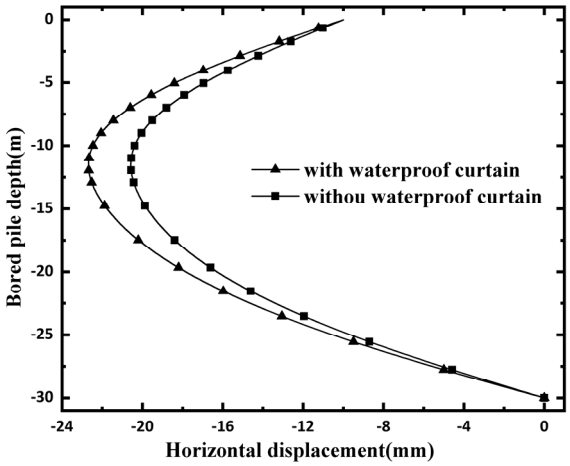


Figure 6. Influence of the waterproof curtain on the horizontal displacement of the pile.

The flow network diagram consists of streamlines intersected by lines of equal head. The arrows are Streamlines, which indicate the direction of flow within the seepage zone. The numbers on the contour lines indicate the water head. Figures 7 and 8 show the flow network diagram with and without waterproof curtain.

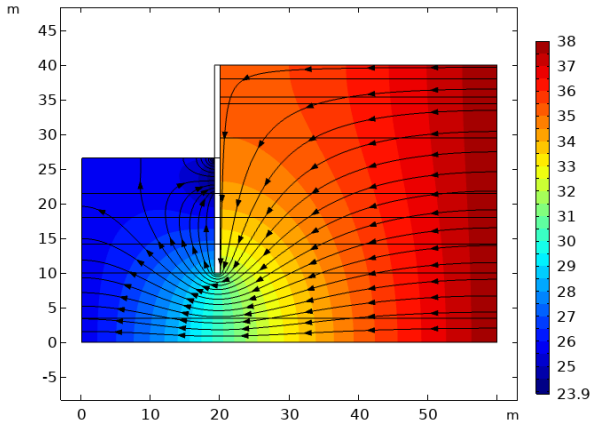


Figure 7. Flow network diagram with waterproof curtain.

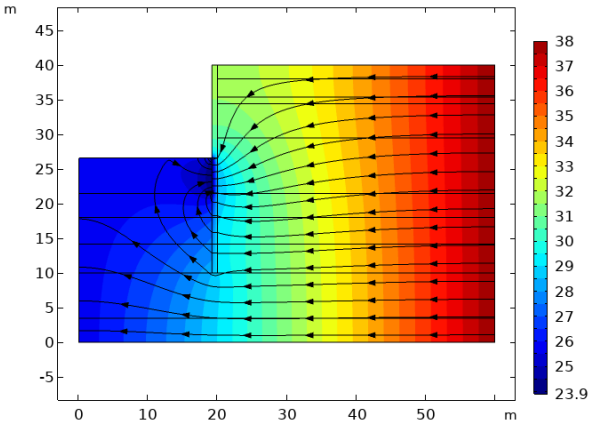


Figure 8. Flow network diagram without waterproof curtain.

In the settlement simulation, it is considered that the whole bored pile is impermeable, and the depth of the waterproof curtain is 30 m. The depth of the waterproof curtain has no effect on the distribution form of the deformation curve of the enclosure structure, but has an effect on the horizontal displacement deformation. Observing the seepage flow network diagram of the foundation pit, with the setting of the waterproof curtain, the ground settlement is significantly reduced, but the disadvantage is that the deformation of the waterproof curtain enclosure structure of the bored pile is larger. This is close to the actual law of engineering, and is in line with the experimental research conclusions of Zhang [9] and Chen [10].

The distribution characteristics of the two flow network diagrams are different. Under the condition that the pumping rate of the precipitation well remains unchanged and the boundary conditions remain unchanged, the installation of the water barrier changes the seepage path, the direction of seepage outside the pit changes from pointing towards the bored pile to pointing towards the bottom of the water barrier, and the seepage rate is significantly reduced. Secondly, the iso-head line changes from around the precipitation well to around the bottom of the curtain, resulting in a thin distribution of iso-head lines outside the pit and a reduction in pore pressure, which is the reason for the reduction in settlement after the installation of the curtain. In the case of setting the waterproof curtain, the seepage flow lines of the foundation pit all surround the bottom of the waterproof curtain, and are generally distributed in a "U" shape, with equal water head lines separated by the bottom of the water curtain is surrounded by a circle center, and the distribution outside the pit is not dense and uneven. In the case of no waterproof curtain, the seepage flow line of the foundation pit is concentrated at the precipitation height of the dewatering well in the foundation pit, and the iso-water head line is surrounded by this position as

the center, and the iso-water head line is evenly distributed and has no obvious dispersion outside the pit. It is not difficult to draw a conclusion that after setting the waterproof curtain, the pore water pressure on the right side of the bored pile is greater than that without the curtain, while the pore water pressure on the left side of the bored pile is similar. The horizontal displacement of bored piles is larger.

5. Influence of Permeability Coefficient in Aquitard

With the change of the permeability coefficient of the aquitard, the settlement outside the pit will change accordingly. The silty clay layer of this model is an aquitard, the permeability coefficient is the empirical parameter value of silty clay, and the horizontal permeability coefficient is 5×10^{-4} m·d^{-1}, vertical permeability coefficient is 1×10^{-4} m·d^{-1}. The permeability coefficient was chosen with reference to the parameters in study [24], and numerical simulations revealed that the amount of change in displacement was only observable when the permeability coefficient was changed ten times over. The main parameter of the aquitard is that its permeability coefficient is much lower than that of the confined aquifer. Impermeable layer seepage is blocked. Exponentially increase or decrease the permeability coefficient of the aquitard, calculate in groups, and consider the horizontal permeability coefficient and the vertical permeability coefficient increased 10, 100, and 1000 times to form four groups. The analysis of the two situations with or without the waterproof curtain was considered separately, and the role of the waterproof curtain in the case of different permeability coefficients of aquitards was explored. This chapter analyzes the changes of flow network diagrams with different permeability coefficient to explain the changing laws of horizontal displacement and settlement.

5.1. Deformation Simulation with Waterproof Curtain

Figure 9 shows the change of horizontal displacement of bored piles with the change of permeability coefficient, and Figure 10 shows the change of settlement amount with the change of permeability coefficient. Figures 11 and 12 are flow network diagrams of foundation pits with different permeability coefficients. All of the above are with a waterproof curtain. The research conclusion shows that the increase of the permeability coefficient of the weakly permeable layer leads to the decrease of the horizontal displacement and the increase of the surface settlement. It is easy to find out by observing the flow network diagram:

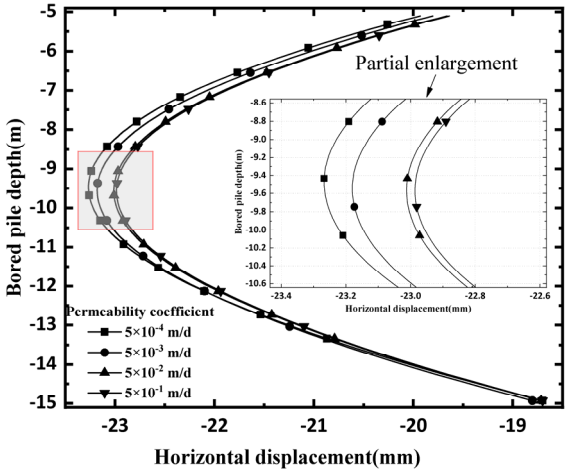


Figure 9. Horizontal displacement of different permeability coefficients with waterproof curtain.

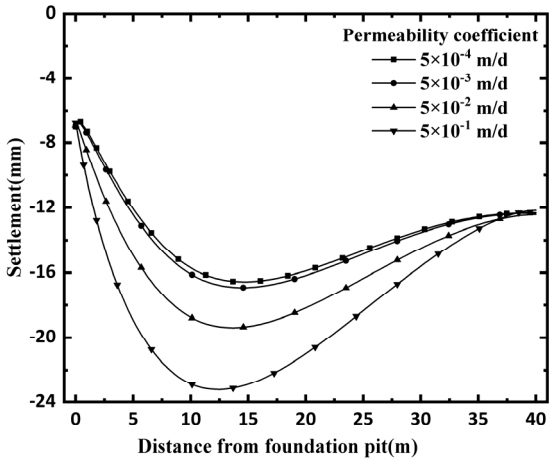


Figure 10. Settlement of different permeability coefficients without waterproof curtain.

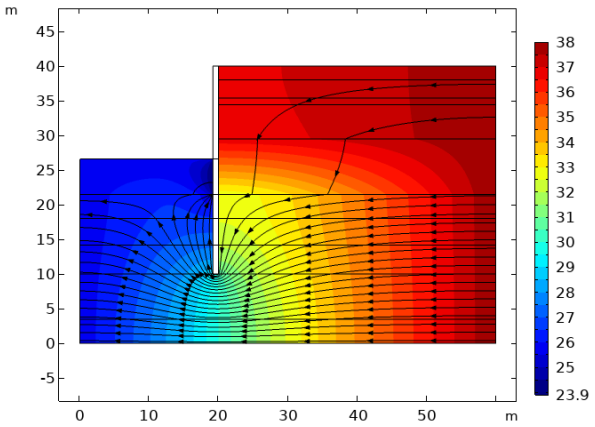


Figure 11. Flow network diagram with permeability coefficient of 5×10^{-2} m·d^{-1}.

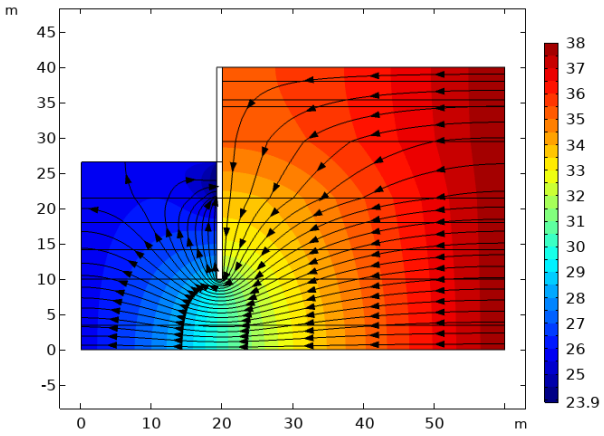


Figure 12. Flow network diagram with permeability coefficient of 5×10^{-1} m·d^{-1}.

(1) The interval between the iso-water head lines in the upper area of the weakly permeable layer is larger than that in the lower part, and the water head at the same position increases while the pressure head decreases. The smaller the permeability coefficient of the weakly permeable layer, the larger the interval distance between the isohydraulic lines, and the larger the water head at the same position, which is considered to be the reason for the reduction of the surface settlement outside the pit.

(2) As the permeability coefficient of the aquitard decreases, the iso-water head line shifts at the boundary of the aquitard, the seepage curve occurs and the seepage obstruction

increases, the curve is not dense, the smaller the permeability coefficient of the aquitard, the offset angle bigger.

(3) After the permeability coefficient of the weakly permeable layer increases, both the horizontal and vertical seepage increase, and the increase is obvious near the bored pile. The seepage velocity in the lower part of the weakly permeable layer is obviously higher than that in the upper part. The weakly permeable layer will cause the pore water pressure on the left and right sides of the bored pile to increase, while the pore water pressure on the left side increases more, and the pore water pressure on the right side increases less. It is considered that this is the reason why the horizontal displacement of bored piles increases as the permeability coefficient decreases. In this model, the weakly permeable layer is located just near the precipitation height of the foundation pit, and has the characteristics of downward seepage in the upper part and upward seepage in the lower part.

5.2. Deformation Simulation without Waterproof Curtain

Figure 13 shows the change of the horizontal displacement of the bored pile with the change of the permeability coefficient, and Figure 14 shows the change of the settlement with the change of the permeability coefficient. Figures 15 and 16 are flow network diagrams of foundation pits with different permeability coefficients. The research results show that, the permeability coefficient of the weakly permeable layer and the horizontal displacement increase and the surface settlement decreases when there is no waterproof curtain. Observe the flow network diagram and find:

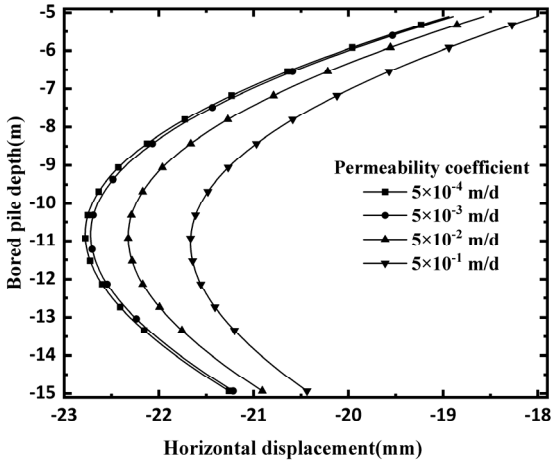


Figure 13. Horizontal displacement of different permeability coefficients without waterproof curtain.

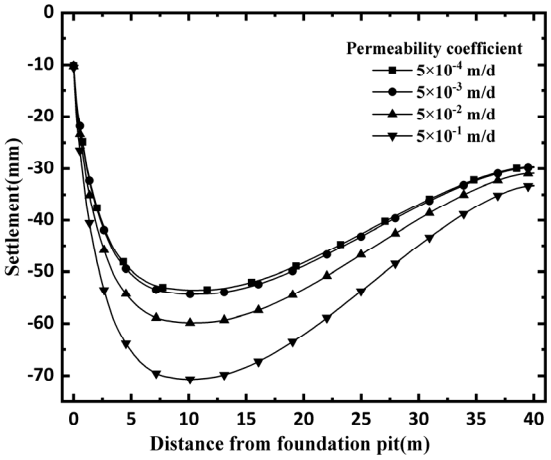


Figure 14. Settlement of different permeability coefficients without waterproof curtain.

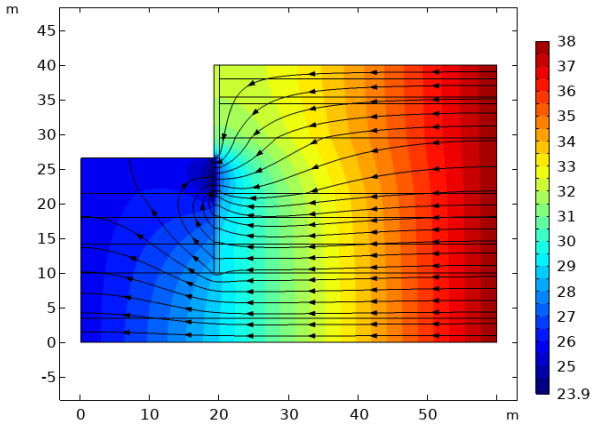


Figure 15. Flow network diagram with permeability coefficient of 5×10^{-1} m·d^{-1}.

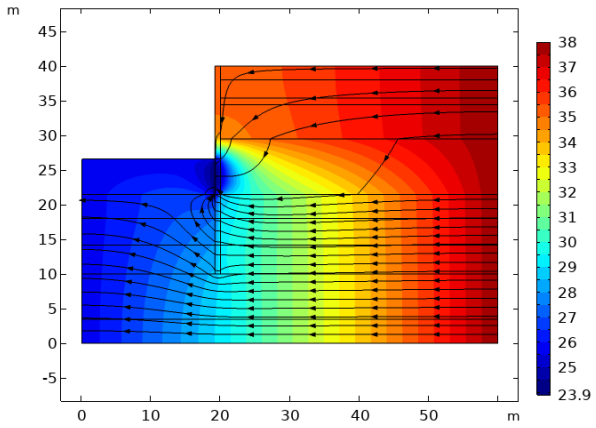


Figure 16. Flow network diagram with permeability coefficient of 5×10^{-2} m·d^{-1}.

(1) First, the law of seepage changes, and the direction changes from a "U"-shaped distribution around the bottom of the waterproof curtain to concentrated in the precipitation position. The water head line also has the characteristics of the previous section: the smaller the permeability coefficient of the aquitard, the greater the distance between the water head lines, and the greater the water head at the same position.

(2) The water head line is shifted in the area of the aquitard, and is surrounded by the precipitation height of the foundation pit as the center. The smaller the water head, the smaller the surrounding radius, and the smaller the surrounding radius at the aquitard.

(3) The waterproof curtain effectively reduces the influence of the weakly permeable layer on the deformation of the foundation pit. Whether it is the horizontal displacement of the bored pile or the surface settlement outside the pit, the deformation when there is a waterproof curtain is smaller than that without the waterproof curtain.

6. Conclusions

(1) The horizontal displacement of bored piles and the surface settlement are important indicators to measure the stability of foundation pit engineering. However, considering the seepage effect of dewatering excavation in numerical simulation is closer to the actual situation of the project, which can effectively improve the accuracy of the numerical simulation. The study found that the calculated value of the fluid-solid coupling model is generally larger than that of the single case only considering soil plasticity, and is closer to the actual monitoring value. By analyzing the calculated values of the shear stress and von Mises stress distribution of the bored pile, there is a sudden change of shear stress at the junction of the pit bottom and the bored pile, and the monitoring and protection of this position should be strengthened.

(2) The influence of the waterproof curtain on the deformation of the foundation pit: the setting of the waterproof curtain has an influence on the seepage direction, which reduces the surface settlement significantly, and the disadvantage is that the horizontal displacement of the bored piles increases. Summarizing the distribution law of the flow network diagram and analyzing the causes of deformation, the pore water pressure on the right side of the bored pile increases while the pore water pressure on the left side is almost unchanged.

(3) The influence of the seepage velocity of the aquitard on the settlement and pore water pressure of the aquitard: This research shows that, the aquitard will lead to an increase in the horizontal displacement and a decrease in the surface settlement. And surround the circle with the precipitation height of the foundation pit as the center. The smaller the position of the water head, the smaller the surrounding radius. In addition, the waterproof curtain effectively reduces the influence of the weak water permeable layer on the deformation of the foundation pit.

Author Contributions: Data curation, Y.Z.; Formal analysis, Z.J.; Funding acquisition, Y.Z. and B.H.; Methodology, Z.J. and Y.Z.; Software, Y.H.; Supervision, C.N. and Z.J.; Writing—original draft, Z.J. and Y.Z.; writing—review and editing, Z.J. and Y.Z. All authors have read and agreed to the published version of the manuscript.

Funding: This research was supported by a grant from the Natural Science Foundation of Gansu province (No.22JR5RA326), Double-First Class Major Research Programs, Educational Department of Gansu Province (No. GSSYLXM-04), Gansu Provincial Department of Natural Resources Science and Technology innovation talent cultivation Project (2022-09). This support is much appreciated.

Institutional Review Board Statement: Not applicable.

Informed Consent Statement: Not applicable.

Data Availability Statement: Data will be made available on request.

Acknowledgments: The authors thank the funding agency and the anonymous reviewers for their recognition of this study.

Conflicts of Interest: The authors declare no conflict of interest.

References

1. Li, X. Completely coupled analysis of seepage field and stress field in deep foundation pit based on displacement back analysis. *Chin. J. Rock Mech. Eng.* **2004**, *23*, 1269–1274.
2. Fearnhead, N.; Maniscalco, K.; Standing, J.R.; Wan, M. Deep excavations: Monitoring mechanisms of ground displacement. *Geotech. Eng.* **2015**, *167*, 117–129. [CrossRef]
3. Shen, S.L.; Xu, Y.S. Numerical evaluation of land subsidence induced by groundwater pumping in Shanghai. *Can. Geotech. J.* **2011**, *48*, 1378–1392. [CrossRef]
4. Xu, X.B.; Hu, Q.; Huang, T.M.; Chen, Y.; Shen, W.M.; Hu, M.Y. Seepage failure of a foundation pit with confined aquifer layers and its reconstruction. *Eng. Fail. Anal.* **2022**, *138*, 106366. [CrossRef]
5. Zhang, Z.; Liu, M.; Zhou, M.; Chen, J. Dynamic Reliability Analysis of Nonlinear Structures Using a Duffing-system-based Equivalent Nonlinear System Method. *Int. J. Approx. Reason.* **2020**, *126*, 84–97. [CrossRef]
6. Zhang, Z.; Li, W.; Yang, J. Analysis of stochastic process to model safety risk in the construction industry. *J. Civ. Eng. Manag.* **2021**, *27*, 87. [CrossRef]
7. Liu, J.; Chen, J.; Wang, J. Fluid-solid coupling analysis of multi-step precipitation in Hongqiao transportation hub. *Chin. J. Geotech. Eng.* **2013**, *35*, 210–215.
8. Xue, L.Y.; Yang, B.; Liu, F.; Zhang, B.; Wang, K. Research on groundwater seepage model test system for foundation pit engineering. *Chin. J. Geotech. Eng.* **2017**, *39*, 126–131. [CrossRef]
9. Zhang, Z.; Guo, Y.; Fan, Q.; Zhang, Q. Calculation method of ground subsidence outside the pit caused by precipitation of foundation pit with suspended water-stop curtain. *J. Northeast. Univ. (Nat. Sci. Ed.)* **2021**, *9*, 1329–1334. [CrossRef]
10. Chen, L.; Zhu, D.; Yang, C.; Xu, C. Influence of water-proof curtain on deformation control of deep foundation pit dewatering excavation. *Chin. J. Civ. Environ. Eng.* **2021**, *4*, 24–32.
11. Shen, S.L.; Wu, Y.X.; Misra, A. Calculation of head difference at two sides of a cut-off barrier during excavation dewatering. *Comput. Geotech.* **2017**, *91*, 192–202. [CrossRef]

12. Yuan, C.; Hu, Z.; Zhu, Z.; Yuan, Z.; Fan, Y.; Guan, H.; Li, L. Numerical simulation of seepage and deformation in excavation of a deep foundation pit under water-rich fractured intrusive rock. *Geofluids* **2021**, *2021*. [CrossRef]
13. Xu, Y.S.; Ma, L.; Shen, S.L.; Du, Y.J. Geological and hydrogeological environment in shanghai with geohazards to construction and maintenance of infrastructures. *Eng. Geol.* **2009**, *109*, 241–254. [CrossRef]
14. Wu, Y.X.; Shen, S.L.; Lyu, H.M.; Zhou, A. Analyses of leakage effect of waterproof curtain during excavation dewatering. *J. Hydrol.* **2020**, *583*, 124582. [CrossRef]
15. Wu, Y.X.; Lyu, H.M.; Han, J.; Shen, S.L. Dewatering-induced building subgrade settlement around a deep excavation in soft deposit in tianjin, china. *J. Geotech. Geoenviron. Eng.* **2019**, *145*, 05019003. [CrossRef]
16. Voottipruex, P.; Jamsawang, P.; Sukontasukkul, P.; Jongpradist, P.; Horpibulsuk, S.; Chindaprasirt, P. Performances of SDCM and DCM walls under deep excavation in soft clay: Field tests and 3D simulations. *Soils Found.* **2019**, *59*, 1728–1739. [CrossRef]
17. Shen, S.L.; Ma, L.; Xu, Y.S.; Yin, Z.Y. Interpretation of increased deformation rate in aquifer iv due to groundwater pumping in shanghai. *Can. Geotech. J.* **2013**, *50*, 1129–1142. [CrossRef]
18. Tian, R.; Zhang, Y.; Xu, A.; Li, X.; Hou, Y.; Tai, B. Impact of Cooling on Water and Salt Migration of High-Chlorine Saline Soils. *Geofluids* **2021**, *2021*. [CrossRef]
19. Wang, X.W.; Yang, T.L.; Xu, Y.S.; Shen, S.L. Evaluation of optimized depth of waterproof curtain to mitigate negative impacts during dewatering. *J. Hydrol.* **2019**, *577*, 123969. [CrossRef]
20. Tan, Y.; Lu, Y.; Wang, D. Deep excavation of the Gate of the Orient in Suzhou stiff clay: Composite earth-retaining systems and dewatering plans. *J. Geotech. Geoenviron. Eng.* **2018**, *144*, 05017009. [CrossRef]
21. Zheng, G.; Tong, J.; Zhang, T.; Wang, R.; Fan, Q.; Sun, J.; Diao, Y. Experimental study on surface subgrade settlements induced by sequential excavation of two parallel tunnels in drained granular soil. *Tunn. Undergr. Space Technol.* **2020**, *103347*, 1–11.
22. Xu, Y.-S.; Ma, L.; Shen, S.-L.; Sun, W.-J. Evaluation of land subsidence by considering underground structures that penetrate the aquifers of shanghai, china. *Hydrogeol. J.* **2012**, *20*, 1623–1634. [CrossRef]
23. Wang, J.; Wang, P.; Wang, W.; Zhou, S.; Fang, X. Optimization analysis of deformation of underlying tunnel in dewatering and excavation of phreatic aquifer. *Adv. Mater. Sci. Eng.* **2019**, *2019*, 1–15. [CrossRef]
24. Liu, X.-X.; Shen, S.-L.; Xu, Y.-S.; Yin, Z.-Y. Analytical approach for time-dependent groundwater inflow into shield tunnel face in confined aquifer. *Int. J. Numer. Anal. Methods Geomech.* **2018**, *42*, 655–673. [CrossRef]
25. Ni, X.; Lu, J.; Wang, C.; Huang, S.; Tang, D. Systematic Analysis Method for the Unusual Large Displacement in the Excavations in Soft Soil Area. *Math. Probl. Eng.* **2021**, *2021*. [CrossRef]
26. Zheng, G.; Ha, D.; Loaiciga, H.; Zhou, H.; Zeng, C.; Zhang, H. Estimation of the hydraulic parameters of leaky aquifers based on pumping tests and coupled simulation/optimization: Verification using a layered aquifer in Tianjin, China. *Hydrogeol. J.* **2019**, *27*, 3081–3095. [CrossRef]
27. Li, J. A nonlinear elastic solution for 1-D subsidence due to aquifer storage and recovery applications. *Hydrogeol. J.* **2003**, *11*, 646–658. [CrossRef]
28. Mahariq, I.; Kurt, H. Strong field enhancement of resonance modes in dielectric microcylinders. *JOSA B* **2016**, *33*, 656–662. [CrossRef]
29. Mahariq, I.; Kuzuoğlu, M.; Tarman, I.H.; Kurt, H. Photonic nanojet analysis by spectral element method. *IEEE Photonics J.* **2014**, *6*, 1–14. [CrossRef]
30. Yazgan-Birgi, P.; Arafat, H.A.; Ali, M.I.H. Implementation of two multiphase flow methods in modeling wetting of microporous hydrophobic membranes. *Sci. Total Environ.* **2019**, *691*, 1251–1261. [CrossRef]
31. Biot, M.A. General theory of three-dimensional consolidation. *J. Appl. Phys.* **1941**, *12*, 155–164. [CrossRef]
32. Teatini, P.; Ferronato, M.; Gambolati, G.; Gonella, M. Groundwater pumping and land subsidence in the Emilia-Romagna coastland, Italy: Modeling the past occurrence and the future trend. *Water Resour. Res.* **2006**, *42*. [CrossRef]
33. Yang, J.; Yang, D.; Han, H.; Qiu, L.; Cheng, Y. A wave propagation model with the Biot and the fractional viscoelastic mechanisms. *Sci. China Earth Sci.* **2021**, *64*, 364–376. [CrossRef]
34. Selvadurai, A.P.S.; Suvorov, A.P. Coupled hydro-mechanical effects in a poro-hyperelastic material. *J. Mech. Phys. Solids* **2016**, *91*, 311–333. [CrossRef]
35. Jiang, H.; Jiang, A.; Xu, M. Research on Algorithm and Coupling Damage Model of Rock Under High Temperature and Loading Based on Mohr–Coulomb Criterion. *Int. J. Comput. Methods* **2022**, *19*, 2250001. [CrossRef]
36. Coelho, P.G.; Barroca, B.C.; Conde, F.M.; Guedes, J.M. Minimization of maximal von Mises stress in porous composite microstructures using shape and topology optimization. *Struct. Multidiscip. Optim.* **2021**, *64*, 1781–1799. [CrossRef]
37. Khatri, V.N.; Kumar, J. Bearing capacity factor Nc under ϕ= 0 condition for piles in clays. *Int. J. Numer. Anal. Methods Geomech.* **2009**, *33*, 1203–1225. [CrossRef]
38. Chakraborty, D.; Kumar, J. Use of von Mises yield criterion for solving axisymmetric stability problems. *Geomech. Geoengin.* **2015**, *10*, 234–241. [CrossRef]
39. Wang, J.; Xu, H.; Xu, D.; Du, P.; Zhou, Z.; Yuan, L.; Cheng, X. Accelerated carbonation of hardened cement pastes: Influence of porosity. *Constr. Build. Mater.* **2019**, *225*, 159–169. [CrossRef]